Free vibration analysis of functionally graded porous materials complex shells with variable thickness

Farzaneh Jafari Maryaki, Alireza Shaterzadeh*

Faculty of Mechanical Engineering, Shahrood University of Technology, Shahrood, Iran

* Corresponding author, Email: a_shaterzadeh@shahroodut.ac.ir

Abstract

This research investigates the vibration characteristics of composite shells featuring a cylindrical-hemispherical geometry, fabricated from functionally graded porous materials with varying thicknesses. Two kind of boundary conditions are assumed: the first assumes both ends are free, while the second involves clamped and free edges for the cylindrical and hemispherical sections, respectively. The analysis employs three-dimensional elasticity principles in conjunction with the Ritz method, utilizing orthogonal polynomials like Legendre polynomials as admissible functions. The natural frequencies' convergence is demonstrated, and results are validated against prior findings from finite element and analytical methods. After confirming the model's accuracy, the influence of porosity is examined. The results indicate that a higher percentage of porosity leads to a decrease in the shell's natural frequencies. The study also investigates how natural frequencies are affected by various geometric parameters. Ultimately, the outcomes highlight the significant impact of porosity and geometric attributes on the frequencies of porous shells. Additionally, torsional and axisymmetric vibration modes are observed to be more influential under clamped-free conditions than under free-free conditions. A general trend of decreasing frequencies with reduced thickness is identified, and higher porosity levels, leading to lower stiffness, consistently reduce frequencies across all modes.

Keywords:

Free vibrations, Functionally graded porous materials, Ritz method, Orthogonal polynomials, Complex shells.

1. Introduction

Shells are extensively utilized across various industries, including automotive, aerospace, submarine, oil, gas, petrochemicals, and refineries. Intricate structural systems frequently experience various forces during their operational lifespan. Vibration analysis helps predict the trend of these structures under various loading and prevents unexpected failures. This is especially important in pressure vessels, heat exchangers, deaerators, reactors, and aerospace structures that are under pressure and temperature. The vibration analysis of these structures can identify the weak points in the design and suggest the necessary corrections to increase the performance and life of the structure and reduce its weight. A major challenge in fabricating of these structures lies in the constraints imposed by material selection and the impact of material properties on structural design. The increasing demand for shells with enhanced mechanical properties has driven researchers to innovate with functionally graded materials (FGMs). These materials offer several advantages, including continuous variation in composition and properties, which mitigate issues at the interface of dissimilar materials. Compared to conventional composite materials, FGMs alleviate thermal and residual stresses as well as stress concentrations, thereby enhancing the structural durability and overall performance. [1]. Functionally graded porous (FGP) materials provide remarkable design flexibility comparable to FGMs while offering distinctive mechanical properties, such as thermal resistance, lightweight characteristics, and excellent energy absorption due to their controlled porosity distribution. Consequently, many researchers have explored the exceptional properties of these materials, leading to a growing body of research in this domain. These studies encompass various structural forms, particularly shells commonly employed in industries, including cylindrical and spherical shells. However, investigations into the vibration behavior of complex structures remain scarce due to the challenges of aligning the connection conditions between substructures. There has been relatively little focus in the existing literature on the vibration analysis of isotropic shells with complex geometries. While studies on simpler shell structures are abundant, detailed investigations into the dynamic behavior of intricate isotropic shells remain scarce. This gap highlights the need for further research to explore how factors such as geometry, boundary conditions, and material properties influence the vibrational characteristics of these

complex systems. Such studies would provide valuable insights for applications in fields like aerospace, automotive, and civil engineering, where complex shell structures are commonly used.

The majority of studies investigating the free vibration behavior of complex shells have concentrated on isotropic materials, leaving FGMs relatively underexplored. While isotropic materials have been extensively analyzed due to their uniform properties, the unique characteristics of FGMs have received limited attention in the context of complex shell vibrations. This disparity underscores a significant research gap, as FGMs offer tailored mechanical properties that could enhance the performance of shells in advanced engineering applications. Further exploration of FGMs in complex shell structures could provide deeper insights into their dynamic behavior and potential benefits. For example, Yegao et al. [2] conducted a dynamic analysis of reinforced cylindrical-conical shells, while in [3], they extended their study to hemispherical-cylindrical-conical shells. These investigations utilized Reissner-Naghdi's shell theory, combined with Fourier series and orthogonal Chebyshev polynomials, to model and analyze the dynamic behavior of these complex shell structures. Their approach provided a robust framework for understanding the vibrational characteristics of such geometries, offering valuable insights into the effects of reinforcement and geometric complexity on dynamic performance. Hamel[4] studied the free vibration of a hemispherical-cylindrical shell using a series solution and obtained accurate results. Tavakoli and Singh[5] proposed the eigenvalue solution of symmetric-hermetic shells based on the normalized Love equations and used ANSYS finite element software to numerically analyze the results. Kang [6-12] developed a three-dimensional analytical approach to determine the free vibration frequencies of cylindrical-conical, hemispherical-cylindrical, and cylindrical-semi-elliptical shells composed of isotropic materials. This method employed the Ritz technique in conjunction with Legendre polynomials to achieve accurate results. Meanwhile, Wu et al. [13-15] investigated the vibrational behavior of spherical-cylindrical-spherical shells using Reissner-Naghdi's shell theory, providing a detailed analysis of the dynamic characteristics of such complex geometries. These studies collectively contribute to a deeper understanding of the vibrational properties of multi-segmented shell structures in various configurations.

Lee [16] presented the dynamic response characteristics of hemispherical, cylindrical and hemispherical-cylindrical shells. The spectral-geometric-Ritz solution for dynamic behavior of spherical -cylindrical-conical shells with various boundary conditions were done by Zhao et al.[17]. They employed the artificial virtual spring technique to model both the boundary conditions and the connection between the two shells. Pang et al. [18] developed a semi-analytical approach for analyzing the dynamic response of spherical-cylindrical-spherical shells with various boundary conditions. Their method, based on the energy method and Flügge thin shell theory, was validated by numerical method and experimental data. Li et al. [19] proposed a semi-analytical technique to examine the dynamic behavior of parabolic-spherical-cylindrical shells using the Ritz method. Their study utilized Flügge theory and employed Fourier series. Lang et al. [20] conducted a semi-analytical investigation of the dynamic characteristics of spherical-cylindrical-spherical interconnected shells with varying thickness. They applied the Ritz method alongside the energy method and first order shear deformation theory (FSDT), validating their findings through comparison with numerical methods. Eslami et al. [21] analyzed the natural frequency properties of functionally graded conical-spherical shells with uniform thickness using the FSDT. They derived the equations of motion and edge constraints through Hamilton's principle and Donnell's theory. Zhang et al. [22] investigated the frequency response of functionally graded porous (FGP) hemispherical-cylindrical-hemispherical shells reinforced with graphene platelets (GPLs). Their analysis utilized 3D elasticity theory, Hamilton's principle, and the finite element method. Sobhani et al. [23] examined the damped dynamic response of tangential waves in functionally graded integrated cylindrical-hemispherical shells. They incorporated synthetic elastic and rotational springs to account for the semi-rigid interface effects between two sections and modeled support flexibility. Using the differential quadrature (DQ) method, they discretized the equations.

Sobhani and Safai [24] performed the first dynamic evaluation of metal-ceramic porous hemispherical-cylindrical shells under elastic boundary conditions. They incorporated a configuration of ten synthetic springs, comprising six translational and four rotational springs, at the shell's ends. The analysis employed

Hamilton's principle and the DQ method to formulate and address the motion equations. Ziyuan et al. [25] introduced a detailed approach to investigate the dynamic behavior of cylindrical-conical shell composite structures under thermal conditions. Using FSDT and thermal strain, they developed the energy equation. The integration of components and the application of diverse support conditions were accomplished using a combined structural methodology, incorporating a virtual spring framework. This approach was executed through the Rayleigh-Ritz technique. Zhou et al. [26] examined the dynamic response of fiber-reinforced cylindrical-conical shells based on classical shell theory. They used synthetic spring technology to represent various support conditions at the interfaces and employed the Rayleigh-Ritz method and the mode combination approach to determine vibration characteristics.

Duke et al. [27] examined the nonlinear dynamic response of a segment of an FG spherical shell in both asymmetric and axially symmetric configurations. The shell rested on an elastic foundation, with various support configurations under thermal condition. The equations of motion were established using the Galerkin technique, with numerical solutions obtained through the Runge-Kutta approach. Li et al. [28] performed a dynamic response analysis of FGP cylindrical shells resting on elastic supports under thermal environments and various edge constraints, utilizing a semi-analytical methodology.

Recently, FGP have been increasingly investigated in structural designs, focusing on components like cylindrical shells [29, 30], beams [31], and plates [32, 33]. Nevertheless, it is worth emphasizing that a significant number of these investigations have not thoroughly examined the influence of pore distribution on the behavior of FGP complex shell structures.

This study introduces several novel advancements in the modeling and analysis of complex shell structures. In contrast to prior methods that treated cylindrical and hemispherical shells independently, this research considers them as a unified structure, improving geometric precision and minimizing computational errors. By utilizing the analytical Ritz method instead of conventional numerical techniques, the study achieves greater accuracy in vibration analysis. Furthermore, the model accounts for spatially varying material

properties and a thickness parameter that varies within the spherical region, providing a more realistic representation of material distributions and practical conditions.

2. Problem formulation

Fig.1 shows a cylindrical-hemispherical shell (C-H shell) made of FGP materials. The surfaces of the hemispherical shell are represented as oval shapes in a cylindrical coordinate feamework *(x, r, θ)*. Here, *x* represents the axial direction, *r* denotes the radial direction, and θ corresponds to the circumferential direction of the shell. The hemispherical shell has a variable thickness *h*, with the radius of the middle surface *R*, and a cylindrical shell with a constant thickness *H* and length *L*. In the analysis of the C-H shell, the cylindrical coordinate as shown in equations (1-*a*) and (1-*b*), to define an integrated and connected shell, we consider its mid-surface, which, for r≥0, rotates 360 degrees around the x-axis. In this structure, the total shell surface is derived by evaluating the volume enclosed between the inner and outer shells. Specifically, the surface of interest is determined by integrating the volumetric difference between these two shells. This method enables a more precise determination of the final shape of the complex shell and offers a cohesive structure for computational analysis [34].

$$x = \sqrt{(R^2 - r^2)} \qquad 0 \le r \le R \tag{1-a}$$

$$r = R \qquad -L \le x \le 0 \tag{1-b}$$

The desired shell region is determined by removing the inner surface geometry from the outer surface geometry.

$$0 \le r \le R - H/2 \quad \& \quad -L \le x \le x_i \quad \& \quad 0 \le \theta \le 2\pi \tag{2-a}$$

$$0 \le r \le R + H/2 \quad \& \quad -L \le x \le x_o \quad \& \quad 0 \le \theta \le 2\pi \tag{2-b}$$

The relation (2-*a*) is the coordinate of the inner shell, and the relation (2-*b*) is the coordinate of the outer shell. where $x_{i,o}$ for $r \ge 0$ are defined by the following equation:

$$x_{i,o} = (R \pm \frac{h}{2}) \sqrt{(1 - \frac{r^2}{(R \pm H/2)^2})} \tag{3}$$

To facilitate mathematical calculations, the *r* and *x* are made dimensionless as defined below:

$$\psi = r/R \quad \& \quad \xi = x/L \tag{4}$$

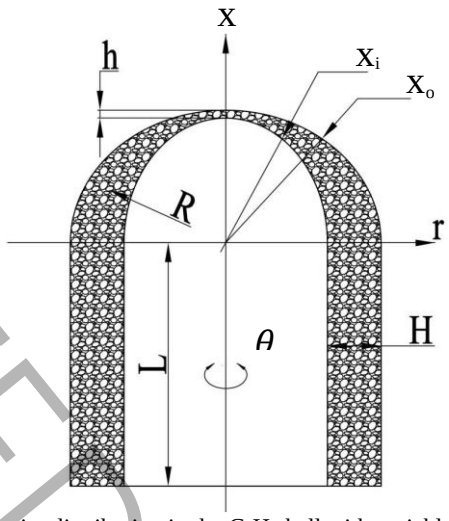

Fig. 1. A view of the geometry and porosity distribution in the C-H shell with variable thickness in cylindrical coordinates *(x, r, θ).*

Therefore, in terms of dimensionless cylindrical coordinates (ξ,ψ,θ), Eq. 2 will be as follows[34].

$$\begin{aligned} &0 \le \psi \le R - H^*/2 \quad \& \quad -1 \le \xi \le \xi_i \quad \& \quad 0 \le \theta \le 2\pi \\ &0 \le \psi \le R + H^*/2 \quad \& \quad -1 \le \xi \le \xi_o \quad \& \quad 0 \le \theta \le 2\pi \end{aligned} \tag{5}$$

that

$$\xi_{i,o} = \frac{x_{i,o}}{L} = \frac{1}{L^*}\left(1 \pm \frac{h^* H^*}{2}\right)\sqrt{1 + \frac{\psi^2}{(1 \pm H^*/2)^2}} \tag{6}$$

where

$$h^* = h/H \quad \& \quad H^* = H/R \quad \& \quad L^* = L/R \tag{7}$$

This study considers the properties of a FGP material for uniform distribution of pores, as shown in Fig 1.

$$\begin{aligned} \rho &= \rho_{\max}\sqrt{1 - e_0\chi} \\ E &= E_{\max}\sqrt{1 - e_0\chi} \\ G &= G_{\max}\sqrt{1 - e_0\chi} \\ \chi &= \left(\frac{1}{e_0} - \frac{1}{e_0}\left(\frac{2}{\pi}\sqrt{1 - e_0} - \frac{2}{\pi} + 1\right)\right)^2 \end{aligned} \tag{8}$$

where

$$e_0 = 1 - \frac{E_{\min}}{E_{\max}} \qquad 0 \le e_0 \le 1 \tag{9}$$

The upper and lower bounds of Young's modulus are designated as $E_{max}\ and,\ E_{min}$, respectively. The maximum shear modulus and mass density are represented by G_{max} and, ρ_{max}, respectively. Finally, e_0 is the porosity coefficient [35, 36].

3. Governing equations

Stress-strain relationship for the graded material as a follow:[37]

$$\begin{Bmatrix} \sigma_{xx} \\ \sigma_{rr} \\ \sigma_{\theta\theta} \\ \sigma_{x\theta} \\ \sigma_{xr} \\ \sigma_{r\theta} \end{Bmatrix} = \frac{E}{(1+\nu)} \begin{bmatrix} \frac{(1-\nu)}{(1-2\nu)} & \frac{\nu}{(1-2\nu)} & \frac{\nu}{(1-2\nu)} & 0 & 0 & 0 \\ \frac{\nu}{(1-2\nu)} & \frac{(1-\nu)}{(1-2\nu)} & \frac{\nu}{(1-2\nu)} & 0 & 0 & 0 \\ \frac{\nu}{(1-2\nu)} & \frac{\nu}{(1-2\nu)} & \frac{(1-\nu)}{(1-2\nu)} & 0 & 0 & 0 \\ 0 & 0 & 0 & \frac{1}{2} & 0 & 0 \\ 0 & 0 & 0 & 0 & \frac{1}{2} & 0 \\ 0 & 0 & 0 & 0 & 0 & \frac{1}{2} \end{bmatrix} \begin{Bmatrix} \varepsilon_{xx} \\ \varepsilon_{rr} \\ \varepsilon_{\theta\theta} \\ \varepsilon_{x\theta} \\ \varepsilon_{xr} \\ \varepsilon_{r\theta} \end{Bmatrix} \tag{10}$$

where, $\{\boldsymbol{\sigma}\}$ represents the stress vector, $\{\boldsymbol{\varepsilon}\}$ denotes the strain vector, and ν is the Poisson's ratio in the FG material. Three-dimensional linear strains $\{\boldsymbol{\varepsilon}\}$ corresponding to three displacements u_x، u_r،u_θ, are defined as follows [29].

$$\begin{aligned} \varepsilon_{xx} &= u_{xx} & 2\varepsilon_{r\theta} &= u_{\theta,r} + \frac{(u_{r,\theta} - u_\theta)}{r} \\ \varepsilon_{rr} &= u_{rr} & 2\varepsilon_{x\theta} &= u_{\theta,x} + \frac{u_{x,\theta}}{r} \\ \varepsilon_{\theta\theta} &= \frac{(u_r + u_{\theta,\theta})}{r} & 2\varepsilon_{xr} &= (u_{r,x} + u_{x,r}) \end{aligned} \tag{11}$$

3-1-Displacement field

The displacement field for complex shells is described as follows:

$$u_x(\psi,\xi,\theta,t) = U_x(\psi,\xi)\cos n\theta \sin(\omega t)$$
$$u_r(\psi,\xi,\theta,t) = U_r(\psi,\xi)\cos n\theta \sin(\omega t)$$
$$u_\theta(\psi,\xi,\theta,t) = U_\theta(\psi,\xi)\sin n\theta \sin(\omega t) \quad (12)$$

U_x, U_r, U_θ are displacement functions depend on ψ, ξ. ω represents the natural frequency, and n indicating the number of circumferential waves. ($n = 0,1,2,\ldots,\infty$). Equation 12 includes all dynamic response modes except torsional mode. [34]. For the torsion mode, $\cos n\theta$ and $\sin n\theta$ should be interchanged in calculations. The displacement functions U_x, U_r, U_θ are assumed to be as follows, which are expressed as Legendre polynomials:

$$U_x(\psi,\xi) = \eta_x(\psi,\xi)\sum_{i=0}^{I}\sum_{j=0}^{J} A_{ij}P_i(\psi)P_j(\xi)$$
$$U_r(\psi,\xi) = \eta_r(\psi,\xi)\sum_{i=0}^{I}\sum_{j=0}^{J} B_{ij}P_i(\psi)P_j(\xi) \qquad i, j = 0,1,2,\ldots$$
$$U_\theta(\psi,\xi) = \eta_\theta(\psi,\xi)\sum_{i=0}^{I}\sum_{j=0}^{J} C_{ij}P_i(\psi)P_j(\xi) \quad (13)$$

In these relations: *(i, j)* are integers and *(I, J)* are the maximum number of sentences used in Legendre polynomial. A_{ij}, B_{ij} *and* C_{ij} are arbitrary coefficients to determine the functions and $\eta_{x,r,\theta}(\psi,\xi)$ are the coefficient of geometric boundary conditions. In completely free boundary conditions (free-free (F-F)) $\eta_x = \eta_r = \eta_\theta = 1$ and in fixed bottom at the end of the cylindrical shell (clamped-free(C-F), $\eta_x = \eta_r = \eta_\theta = \xi + 1$ is considered. [34]

Higher-degree orthogonal polynomials can be employed to address more complex problems, resulting in more accurate frequency calculations. In practice, Mathematical functions with orthogonality properties such as Bessel, Hermite, Laguerre, Chebyshev, and others can be utilized to derive standard sets of compatible basis functions. In the current analysis, Legendre polynomial expansions are chosen as the appropriate trial functions due to their efficiency in terms of computational time, enabling faster results.

$$P_{n+1}(X)=\frac{1}{n+1}\left[(2n+1)XP_n(n)-nP_{n-1}(X)\right] \qquad n=0,1,2,...$$
$$P_0(X)=1, P_1(X)=X, P_2(X)=1/2(3X^2-1), P_3(X)=1/2(5X^3-3X) \tag{14}$$

Legendre polynomials labeled $P_n(X)$ are defined as follows. [34]

4. Analysis of free vibrations

By substituting Eq. (11) into (10), a set of six second-order differential equations is derived in terms of $u_x, u_r \; and \; u_\theta$. The elastic strain energy and energy associated with motion of complex shells can be expressed as follows:

$$V=\frac{1}{2}\iiint\left[\sigma_{xx}\varepsilon_{xx}+\sigma_{rr}\varepsilon_{rr}+\sigma_{\theta\theta}\varepsilon_{\theta\theta}+2(\sigma_{r\theta}\varepsilon_{r\theta}+\sigma_{rx}\varepsilon_{rx}+\sigma_{\theta x}\varepsilon_{\theta x})\right]rdrdxd\theta$$
$$T=\frac{1}{2}\iiint\rho(\dot{u}_x^2+\dot{u}_r^2+\dot{u}_\theta^2)rdrdxd\theta \tag{15}$$

after substituting Eqs. (10) and (11) into Eq. (15), maximum strain and kinetic energies are obtained using dimensionless coordinates ξ and ψ as follows:

$$V_{max}=\frac{1}{2}[\int_0^{1+H^*/2}\int_{-1}^{\xi_0}I_V\psi d\xi d\psi-\int_0^{1-H^*/2}\int_{-1}^{\xi_i}I_V\psi d\xi d\psi]$$
$$T_{max}=\frac{\rho\omega^2LR^2}{2}[\int_0^{1+H^*/2}\int_{-1}^{\xi_0}I_T\psi d\xi d\psi-\int_0^{1-H^*/2}\int_{-1}^{\xi_i}I_T\psi d\xi d\psi] \tag{16}$$

$$I_V=(I_1+I_2+I_3+I_4)\gamma_1+(I_5+I_6)\gamma_2$$
$$I_T=(U_x^2+U_r^2)\gamma_1+(U_\theta^2)\gamma_2 \tag{17}$$

that

$$I_1 = \frac{U_{x,\xi}^2 C_{11}}{L^2} + \frac{2L^* U_{r,\psi} U_{x,\xi} C_{13}}{L^2} + \frac{2L^* U_r U_{x,\xi} C_{12}}{L^2} + \frac{2nL^* U_\theta U_{x,\xi} C_{12}}{L^2}$$

$$I_2 = \frac{L^{*2} C_{22}}{L^2 \psi^2}(U_r^2 + 2nU_r U_\theta + n^2 U_\theta^2)$$

$$I_3 = \frac{2L^{*2} U_r U_{r,\psi} C_{23}}{L^2 \psi} + \frac{2nL^{*2} U_\theta U_{r,\psi} C_{23}}{L^2 \psi} + \frac{L^{*2} U_{r,\psi}^2 C_{33}}{L^2}$$

$$I_4 = \frac{U_{r,\xi}^2 C_{55}}{2L^2} + \frac{L^* U_{r,\xi} U_{x,\psi} C_{55}}{L^2} + \frac{L^{*2} U_{x,\xi}^2 C_{55}}{2L^2}$$

$$I_5 = \frac{U_{\theta,\xi}^2 C_{44}}{2L^2} - \frac{nL^* U_{\theta,\xi} U_x C_{44}}{\psi L^2} + \frac{n^2 L^{*2} U_x^2 C_{44}}{2\psi^2 L^2}$$

$$I_6 = \frac{L^{*2} U_{\theta,\psi}^2 C_{66}}{2L^2} - \frac{nL^{*2} U_{\theta,\psi} U_r C_{66}}{\psi L^2} - \frac{L^{*2} U_{\theta,\psi} U_\theta C_{66}}{\psi L^2} + \frac{n^2 L^{*2} U_r^2 C_{66}}{2\psi^2 L^2} + \frac{nL^{*2} U_r U_\theta C_{66}}{\psi^2 L^2} + \frac{L^{*2} U_\theta^2 C_{66}}{2\psi^2 L^2} \quad (18)$$

and γ_1 and γ_2 are defined as follows.

$$\gamma_1 = \int_0^{2\pi} \cos^2 n\theta d\theta = \begin{cases} 2\pi & \text{if } n = 0 \\ \pi & \text{if } n \geq 1 \end{cases}$$

$$\gamma_2 = \int_0^{2\pi} \sin^2 n\theta d\theta = \begin{cases} 0 & \text{if } n = 0 \\ \pi & \text{if } n \geq 1 \end{cases} \quad (19)$$

The eigenvalue problem is derived by optimizing the energy functional in terms of the unknown parameters A_{ij}, B_{ij} *and* C_{ij}. Increasing the upper limits of (*I, J*) can enhance the accuracy of the resulting frequency response.

$$\frac{\partial}{\partial A_{ij}}(V_{max} - \omega^2 T_{max}^*) = 0$$

$$\frac{\partial}{\partial B_{ij}}(V_{max} - \omega^2 T_{max}^*) = 0 \qquad i = 0,1,2,...,I \quad \& \quad j = 0,1,2,...,J$$

$$\frac{\partial}{\partial C_{ij}}(V_{max} - \omega^2 T_{max}^*) = 0 \quad (20)$$

Here, $T_{\max} = \omega^2 T_{max}^*$ and *(I, J)* are the highest polynomial degrees at which the results converge. As a result, the number of *(I+1) (J+1)* homogeneous linear algebraic equations of A_{ij} , B_{ij}, C_{ij} unknowns are obtained.

This relationship yields a non-trivial solution, other than zero, when the determinant value of the coefficient matrix is set to zero [34].

$$([K]-\Omega^{*}[M])\{Y\}=0 \tag{21}$$

[*K*] and **[*M*]** correspond to the structural stiffness matrix and mass distribution matrix, respectively. Eq. (21) is solved to determine the eigenvalues of the vibrating system. $\Omega^{*}=\frac{R^{2}\omega^{2}\rho}{G}$ is equal to the square of the dimensionless frequency, and the displacement vector is {***Y***}.

$$\{Y\}=\{A_{00},A_{01},\ldots,A_{IJ};B_{00},B_{01},\ldots,B_{IJ};C_{00},C_{01},\ldots,C_{IJ}\}^{T} \tag{22}$$

5. Results

5-1- Convergence and validation of results

To verify the precision of the derived frequencies, it is crucial to perform a numerical evaluation to identify the necessary number of expansion terms in the Legendre polynomial expansion.

In this study, the results were aligned with those from the homogeneous shell analysis presented in reference [29]. Tables 1 and 2 show the results of frequency convergence. Table 1 presents the results for a completely free shell in the torsional mode (n=0^{T}) while Table 2 presents the results for a shell with C-F boundary constraints. i.e., (x = -L) in the axisymmetric mode (n=0^{A}) using Legendre polynomials. The dimensionless frequencies are expressed as $\omega R\sqrt{(\rho/G)}$ To calculate the frequencies, the total number of Legendre polynomial sentences in the axial (*TX*) and radial (*TR*) directions is shown.

The symbols *TX (TX =J+1)* and *TR (TR =I+1)* are the count of Legendre polynomial sentence that are used in the axial (x or ξ) and radial (r or ψ) directions, respectively. The same number of Legendre polynomials is applied in both directions. According to the results shown in Tables 1 and 2, the best convergence of the results occurs at *TR* = 6 and *TX* = 8. To validate the precision of the derived results, the findings of this study are cross-referenced with the data from the reference, as shown in Tables 3-5. The results indicate that the frequencies computed using the 3D Ritz method are consistently lower than those obtained using

2D thin-shell theories that include shear and rotational inertia, which, in turn, provide lower frequencies compared to a 2D analysis that neglects these factors.

Table1. Dimensionless frequencies of a free-free C-H shell with variable thickness ($n=\mathbf{0}^{T}$, *H/R=0.2, h/H=1/3, L/R=0.5*).

		m (mode number)				
TR	*TX*	1	2	3	4	5
3	2	2.679	6.425	17.304	24.497	36.981
	4	2.527	4.324	6.341	10.009	17.552
	6	**2.525**	4.120	5.744	7.845	10.094
	8	2.525	4.115	5.675	7.274	9.190
	10	2.525	4.115	5.666	7.222	8.879
	12	2.525	4.115	5.664	7.213	8.802
4	2	2.678	5.438	10.529	17.500	33.343
	4	2.526	4.193	6.322	8.496	12.009
	6	2.525	**4.114**	5.701	7.287	9.690
	8	2.525	4.115	5.663	7.207	8.828
	10	2.525	4.114	5.662	7.196	8.721
	12	2.525	4.114	**5.661**	7.190	8.714
5	2	2.670	5.279	8.509	14.824	17.167
	4	2.526	4.183	6.087	8.466	10.829
	6	2.525	4.115	5.678	7.280	9.016
	8	2.525	4.114	5.662	7.193	8.730
	10	2.525	4.114	5.661	**7.188**	8.711
	12	2.525	4.114	5.661	7.188	8.700
6	2	2.669	5.190	8.413	11.609	16.103
	4	2.525	4.176	6.076	8.130	10.627
	6	2.525	4.115	5.674	7.243	8.926
	8	2.525	4.114	5.661	7.191	8.721
	10	2.525	4.114	5.661	7.188	8.700
	12	2.525	4.114	5.661	7.188	**8.699**

Table 2. Dimensionless frequencies of a free-free C-H shell with variable ($n=\mathbf{0}^{A}$, *H/R=0.2, h/H=1/3, L/R=0.5*).

		m (mode number)				
TR	*TX*	1	2	3	4	5
4	2	1.557	2.850	2.984	4.667	7.333
	4	1.512	1.645	2.423	2.913	4.251
	6	1.509	1.640	2.095	2.881	3.042
	8	1.508	1.638	2.017	2.809	2.947
	10	1.508	1.637	2.005	2.712	2.924
	12	1.508	1.637	1.999	2.684	2.921
5	2	1.552	2.544	2.955	4.507	7.142
	4	1.511	1.642	2.152	2.912	3.584
	6	1.508	1.638	2.015	2.780	2.930

	8	1.508	1.637	1.999	2.666	2.920
	10	1.508	1.637	1.994	2.647	2.918
	12	1.508	1.637	1.993	2.637	2.917
6	2	1.550	2.017	2.951	4.349	6.492
	4	1.510	1.640	2.115	2.908	3.089
	6	1.508	1.637	2.003	2.701	2.921
	8	1.508	1.637	1.994	2.647	2.918
	10	1.508	1.637	1.992	2.635	2.917
	12	1.508	1.637	1.992	2.630	2.917

Table 3. Dimensionless frequencies of a cylindrical shell (v = 0.2) for different edge constraints.

B.C	*n*	*m*	*L/R*	*H/R*	Present	Ref [38]	Ref [39]	Ref [40]	Ref [41]
F-F	0	1	8.1	0.05	0.372	0.367	0.366	0.367	0.367
F-F	2	5	8.67	0.002	0.431	0.447	0.447	0.447	0.447
F-F	1	1	5	0.002	0.363	----	0.359	0.358	0.358
C-F	2	1	1.14	0.05	0.312	0.307	0.307	0.308	0.308
C-F	2	2	2.88	0.05	0.314	0.308	0.308	0.308	0.308
C-F	2	3	5.07	0.05	0.315	0.307	0.307	0.308	0.308
C-C	4	1	10	0.002	0.015	----	0.0151	0.015	0.015
C-C	2	1	10	0.05	0.059	----	0.059	0.058	0.067
C-C	3	1	0.316	0.05	0.316	----	0.316	0.312	0.318

Table 4. Dimensionless frequency of a clamp-free C-H shell (*h/H=1, H/R = 0.02, v = 0.2*).

	L/R=1		*L/R*=2	
n	Present	Ref [29]	Present	Ref [29]
0^A	2.008	2.006	0.782	----
1	0.918	0.918	0.546	0.546
2	1.580	1.579	0.627	----
3	1.276	1.275	0.638	0.637
4	1.071	1.068	0.535	0.530
5	0.985	0.980	0.569	0.567

Table 5. Dimensionless frequency of a clamp-free C-H shell (*h/H=1, L/R=1, H/R = 0.02, v = 0.2*)

		Series solution	Finite-difference	Finite element		Numerical integration	
n	Present	Ref [4]	Ref [4]	Ref [42]	Ref [42]	Ref [4]	Ref [42]
0^A	2.008	2.058	2.058	2.058	2.058	2.059	2.059
1	0.918	0.943	0.943	0.943	0.943	0.943	0.943
2	1.580	1.609	1.622	1.620	1.620	1.620	1.621
3	1.276	1.306	1.310	1.307	1.307	----	----
4	1.071	1.094	1.097	1.094	1.094	----	----
5	0.985	----	----	----	----	----	----

According to the data presented in the above tables, the obtained results show a good agreement with previous studies. After confirming the correctness of these results, a 3D free vibration analysis of complex shells composed of FGP materials is presented.

4-2-Numerical results

Fig 2 shows the effect of the porosity (e_0 = 0, 0.2, 0.4, 0.6, 0.8) in frequency analysis. In the obtained results, one can see that as the porosity parameter increases in the C-H shell, the frequencies decrease across all modes due to the reduction in stiffness. In the following, the results are presented with *TR* = 6, *TX* = 8, e_0= 0.8, and geometric specifications *H/R*=0.2, *h/H*=1/3 and *L/R* = 0.5. The material properties used in the analysis are as follows:

E=201.04× 10^9 (Pa), ρ=8166 (kg/m^3) and ν =0.3 [43].

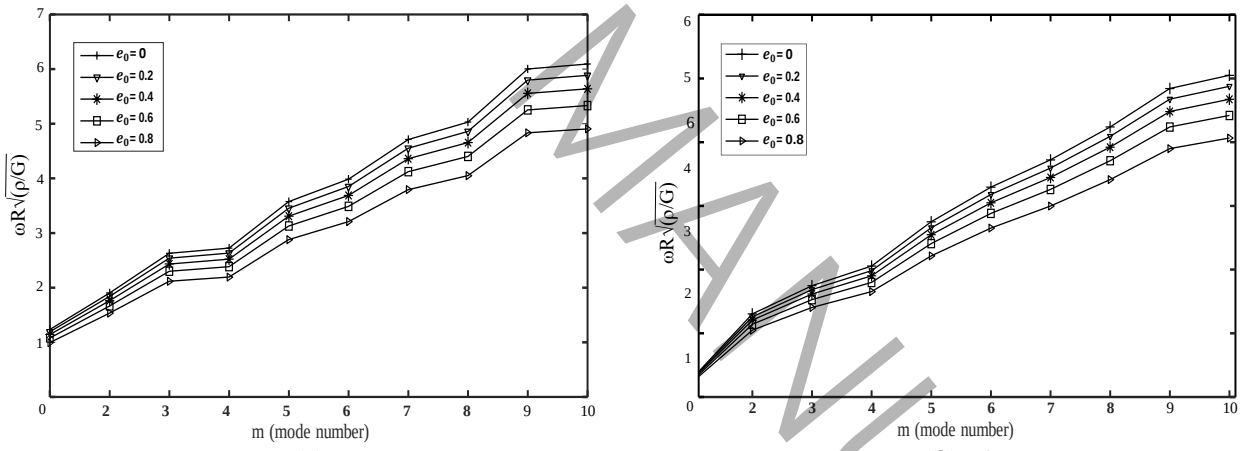

Fig 2. The influence of the porosity parameter on the dimensionless frequencies. a) clamped-free. and b) completely free. (*n* =2)

Superscripts 0^A and 0^T indicate axial and torsional symmetric vibration, respectively. Figure 3 shows that the lowest frequency in all geometries with uniform and variable thickness occurs in free-free boundary conditions at *n* =2 and according to Fig. 4, for a C-F cylindrical shell, the lowest frequency generally occurs at *n* =1. The figures show that the torsional mode (n=0^T) and axisymmetric mode (n=0^A) for C-F are less

compared to the F-F, therefore are more important. Fig. 4 for C-F shows that as the shell thickness (*R/H*) increases, the $n=0^T$ and $n=0^A$ modes are more noticeable.

The results include 35 frequencies for each type of shell geometry, corresponding to seven circumferential wave numbers ($n = 0^A, 0^T$,1,2,3,4,5). Additionally, five mode shapes (m =1,2,3,4,5) are provided for each value of n.

Fig. 3 and 4 illustrate the first five frequencies (minimum values) for each type of structural geometry. The variables (n, m) denote n as the wave number and m as the mode number. For example, in Fig. 3 for the geometry with L/R=1 and H/R=0.1, the first 5 frequencies obtained from the total of 35 frequencies are presented as follows: (0.118(2,1),0.317(3,1),0.583(4,1),0.821(2,2),0.893(3,2)).

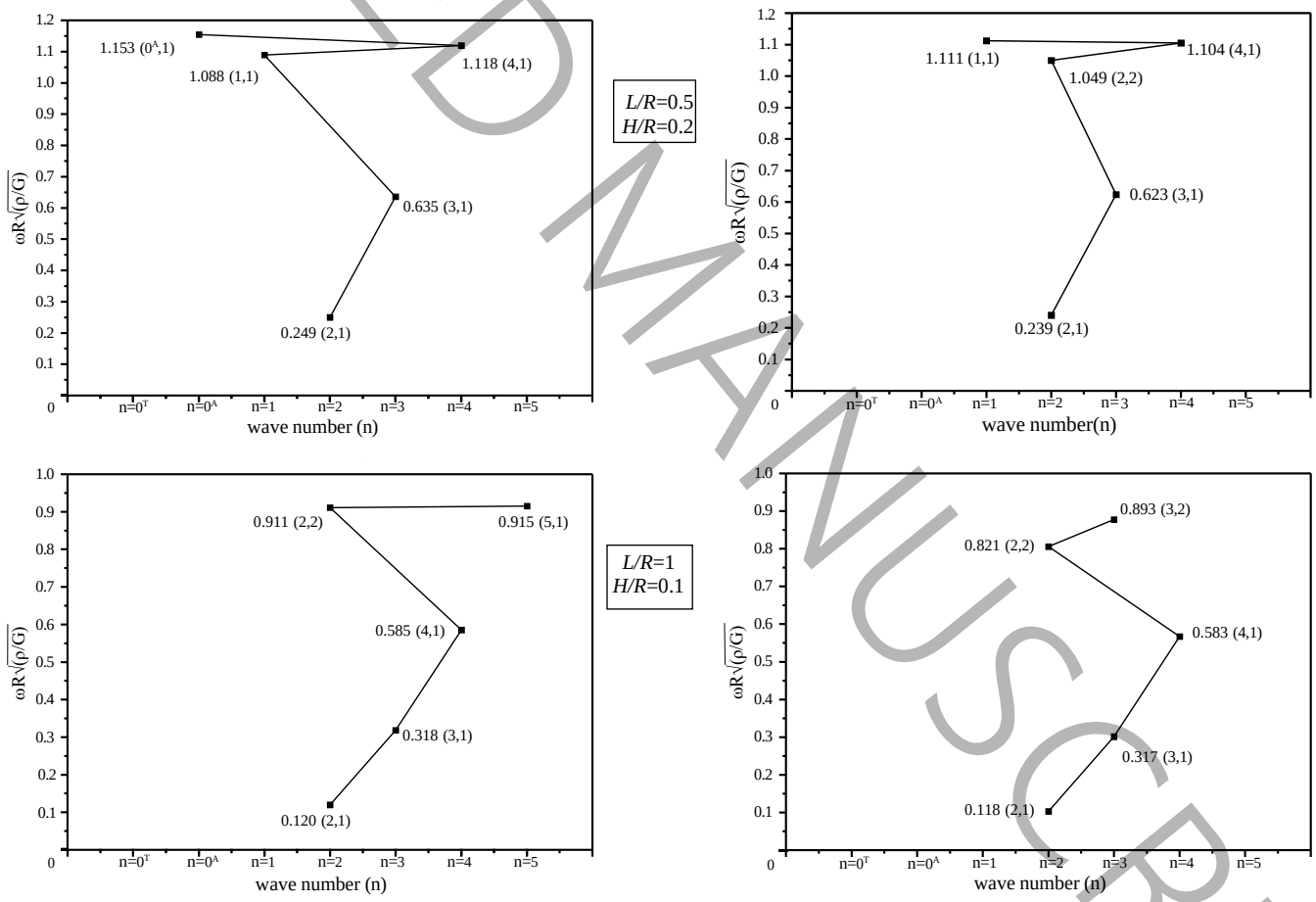

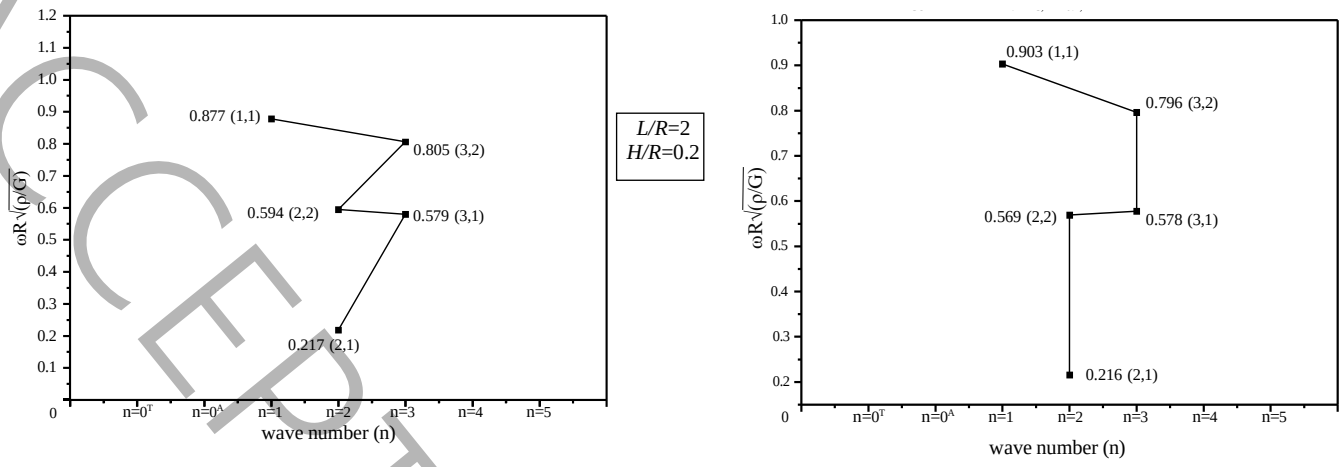

(a) (b)

Fig 3. Dimensionless first 5 frequencies for F-F boundary conditions *a*) uniform (*h*/*H*=1) and, *b*) nonuniform thickness(*h*/*H*=1/3).

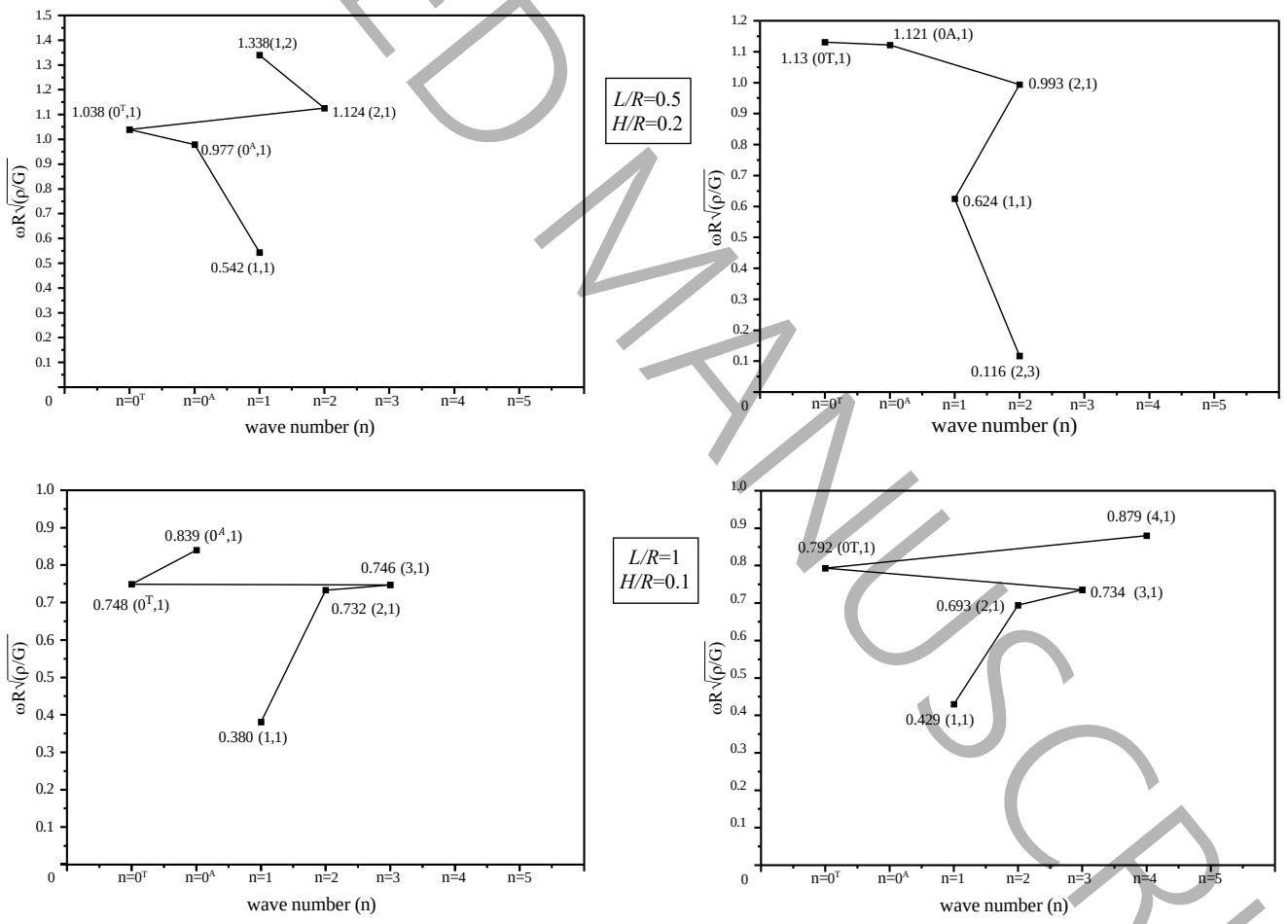

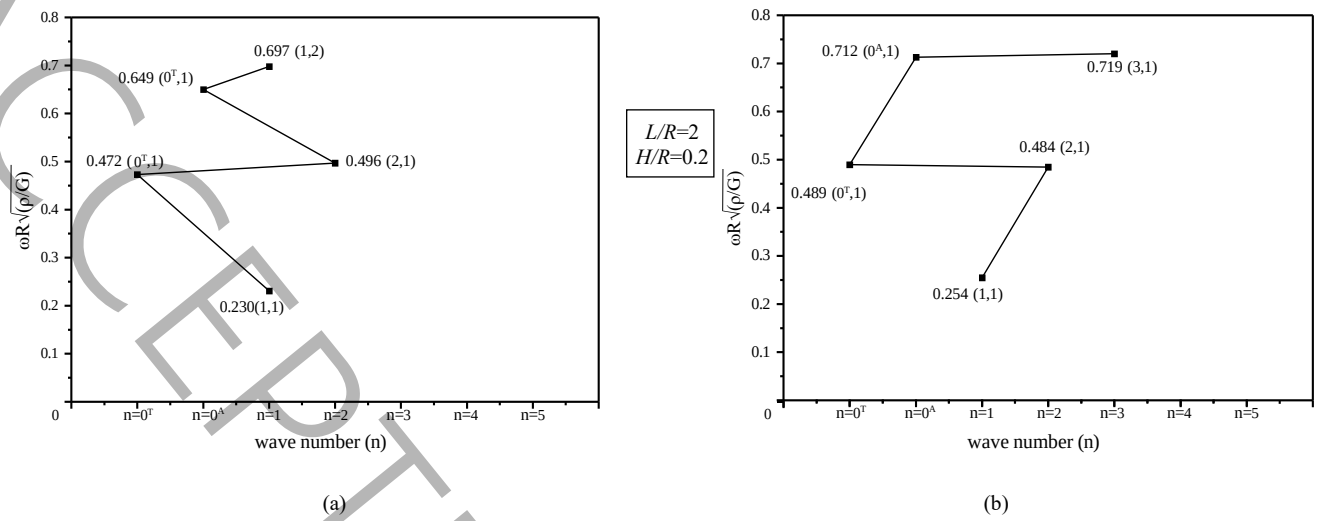

(a) (b)

Fig4: Nondimensional first 5 frequencies in ambient wave n for C-F edge constraints *a*) uniform (*h/H*=1) and, *b*) nonuniform thickness(*h/H*=1/3).

6. Conclusion

Numerical results show distinct patterns in the vibration behavior of FGP C-H shells. For various geometries with constant and non-uniform thickness under free-free edge constraints, the lowest frequency consistently occurs at n =2. On the contrary, at the clamped-free boundary conditions, the lowest frequency occurs at n =1. Further analysis shows that $n=0^T$ and $n=0^A$ have a greater impact in clamped-free compared to free-free boundary conditions. Also, one can observe that with an increase in the porosity parameter in the C-H shell, the frequencies decrease across all modes due to the reduction in stiffness. On the other hand, as expected, decreasing the thickness generally decreases the frequencies in all modes. This study provides a comprehensive analysis of the impact of edge constraints and shell geometry on the dynamic response of cylindrical-hemispherical (C-H) shells. The findings highlight the significance of incorporating edge constraints and geometric characteristics in the development and assessment of such structures to ensure accurate predictions of their dynamic behavior.

7. References

[1] A.R. Shaterzadeh, K. Foroutan, Nonlinear Dynamic Analysis of Eccentrically Stiffened FGM Cylindrical Shells With Elastic Foundation Under Uniform External Pressure, 14 (2016) 11-26. (in persion)

[2] Y. Qu, Y. Chen, X. Long, H. Hua, G. Meng, A modified variational approach for vibration analysis of ring-stiffened conical–cylindrical shell combinations, European Journal of Mechanics-A/Solids, 37 (2013) 200-215.

[3] Y. Qu, S. Wu, Y. Chen, H. Hua, Vibration analysis of ring-stiffened conical–cylindrical–spherical shells based on a modified variational approach, International journal of mechanical Sciences, 69 (2013) 72-84.
[4] J. Hammel, Free vibration of a cylindrical shell with a hemispherical head, 2nd Int. SMiRT Conf. IASMiRT, Raleigh, NC, (1973).
[5] M. Tavakoli, R. Singh, Eigensolutions of joined/hermetic shell structures using the state space method, Journal of Sound and Vibration, 130(1) (1989) 97-123.
[6] J. H. Kang, Three-dimensional vibration analysis of joined thick conical—Cylindrical shells of revolution with variable thickness, Journal of Sound and Vibration, 331(18) (2012) 4187-4198.
[7] J. H. Kang, Free vibrations of combined hemispherical–cylindrical shells of revolution with a top opening, International Journal of Structural Stability and Dynamics, 14(01) (2014) 1350023.
[8] J. H. Kang, Vibration analysis of a circular cylinder closed with a hemi-spheroidal cap having a hole, Archive of Applied Mechanics, 87 (2017) 183-199.
[9] Y. B. Yang, J.-H. Kang, Vibrations of a composite shell of hemiellisoidal-cylindrical shell having variable thickness with and without a top opening, Thin-Walled Structures, 119 (2017) 677-686.
[10] J. H. Kang, Vibrations of a cylindrical shell closed with a hemi-spheroidal dome from a three-dimensional analysis, Acta Mechanica, 228 (2017) 531-545.
[11] J. H. Kang, 3D vibration analysis of hermetic capsules by using Ritz method, International Journal of Structural Stability and Dynamics, 17(03) (2017) 1750040.
[12] J. H. Kang, Three-dimensional vibration analysis of a hermetic capsule with variable thickness, AIAA Journal, 55 (2013) 2093-2102.
[13] S. H. Wu, Y.G. Qu, X.C. Huang, H.X. Hua, Free vibration analysis on combined cylindrical-spherical shell, Applied Mechanics and Materials, 226 (2012) 3-8.
[14] S. Wu, Y. Qu, H. Hua, Vibrations characteristics of joined cylindrical-spherical shell with elastic-support boundary conditions, Journal of mechanical science and technology, 27 (2013) 1265-1272.
[15] S. Wu, Y. Qu, H. Hua, Vibration characteristics of a spherical–cylindrical–spherical shell by a domain decomposition method ,Mechanics Research Communications, 49 (2013) 17-26.
[16] J. Lee, Free vibration analysis of joined spherical-cylindrical shells by matched Fourier-Chebyshev expansions, International Journal of Mechanical Sciences, 122 (2017) 53-62.
[17] Y. Zhao, D. Shi ,H. Meng, A unified spectro-geometric-Ritz solution for free vibration analysis of conical–cylindrical–spherical shell combination with arbitrary boundary conditions, Archive of Applied Mechanics, 87 (2017) 961-988.
[18] H. Li, F. Pang, Y. Ren, X. Miao, K .Ye, Free vibration characteristics of functionally graded porous spherical shell with general boundary conditions by using first-order shear deformation theory, Thin-Walled Structures, 144 (2019) 106331.
[19] H. Li, F. Pang, X. Wang, Y. Du, H. Chen, Free vibration analysis of uniform and stepped combined paraboloidal, cylindrical and spherical shells with arbitrary boundary conditions, International Journal of Mechanical Sciences, 145 (2018) 64-82.
[20] H. Li, G. Cong, L. Li, F. Pang, J. Lang, A semi analytical solution for free vibration analysis of combined spherical and cylindrical shells with non-uniform thickness based on Ritz method, Thin-Walled Structures, 145 (2019) 106443.
[21] H. Bagheri, Y. Kiani, M. Eslami, Free vibration of FGM conical–spherical shells, Thin-Walled Structures, 160 (2021) 107387.
[22] D. Zhang, Y. Wang, L. Li, Free vibration response of FG porous joined hemispherical–cylindrical–hemispherical shell vessels reinforced by graphene platelet, International Journal of Structural Stability and Dynamics, 23 (2023) 2350025.
[23] E. Sobhani, A.R. Masoodi, Ö. Civalek, A.R. Ahmadi-Pari, Free-damped vibration tangential wave responses of FG-sandwich merged hemispherical-cylindrical shells under effects of artificial springs at merging and boundary conditions, Engineering Structures, 284 (2023) 115958.
[24] E. Sobhani, B. Safaei, Dynamical characteristics of fastening of a cylindrical shell with a hemispherical shell made of graded porous power ceramic-metal under elastic boundary edges, Engineering Analysis with Boundary Elements, 156 (2023) 432-454.
[25] Z. Zhu, Y. Zhang, R. Xu, L. Zhao, G. Wang, Q. Liu, Analysis of thermal-vibration coupling modeling of combined conical-cylindrical shell under complex boundary conditions, Journal of Vibration and Control, 30(15-16) (2024) 3377-3387.
[26] Z. Xu, X.-C. Yu, H. Li, P.-Y. Xu, X.-C. Sun, Y.-F. Zhang, D.-W. Gu, Q.-K. Han, B.-C. Wen, The Vibration Characteristics Analysis of Fiber-Reinforced Thin-Walled Conical–Cylindrical Composite Shells with Artificial Spring Technique, International Journal of Structural Stability and Dynamics, (2024) 2550200.

[27] N.D. Duc, V.D. Quang, V.T.T. Anh, The nonlinear dynamic and vibration of the S-FGM shallow spherical shells resting on an elastic foundations including temperature effects, International Journal of Mechanical Sciences, 123 (2017) 54-63.
[28] H. Li, F. Pang, H. Chen, Y. Du, Vibration analysis of functionally graded porous cylindrical shell with arbitrary boundary restraints by using a semi analytical method, Composites Part B: Engineering, 164 (2019) 249-264.
[29] K. Xie, M. Chen, An analytical method for free vibrations of functionally graded cylindrical shells with arbitrary intermediate ring supports, Journal of the Brazilian Society of Mechanical Sciences and Engineering, 43 (2021) 1-24.
[30] F. Kiani, M. Hekmatifar, D. Toghraie, Analysis of forced and free vibrations of composite porous core sandwich cylindrical shells and FG-CNTs reinforced face sheets resting on visco-Pasternak foundation under uniform thermal field, Journal of the Brazilian Society of Mechanical Sciences and Engineering, 42(10) (2020) 504.
[31] A.A.P. Zanoosi, Size-dependent thermo-mechanical free vibration analysis of functionally graded porous microbeams based on modified strain gradient theory, Journal of the Brazilian Society of Mechanical Sciences and Engineering, 42(5) (2020) 236.
[32] R. Ansari, M.Z. Ershadi, A. Mirsabetnazar, M.F. Oskouie, Nonlinear large amplitude vibrations of annular sector functionally graded porous composite plates under instantaneous hygro-thermal shock, Journal of the Brazilian Society of Mechanical Sciences and Engineering, 46(9) (2024) 541.
[33] W. Zhao, X. Gong, D. Guo, C. Li, Free vibration and thermal buckling analysis of FGM sandwich circular plate under transverse non-uniform temperature rise, Journal of the Brazilian Society of Mechanical Sciences and Engineering, 46(2) (2024) 108.
[34] J.-H. Kang, Vibrations of complex shells with variable thickness, Journal of Engineering Mechanics, 143(8) (2017) 04017053.
[35] D.H. Bich, D.G. Ninh, T.I. Thinh, Non-linear buckling analysis of FGM toroidal shell segments filled inside by an elastic medium under external pressure loads including temperature effects, Composites Part B: Engineering, 87 (2016) 75-91.
[36] D.G. Ninh, D.H. Bich, Nonlinear buckling of eccentrically stiffened functionally graded toroidal shell segments under torsional load surrounded by elastic foundation in thermal environment, Mechanics Research Communications, 72 (2016)1-15.
[37] T.N. Doan, A.T. Nguyen, P. Van Binh, T. Van Hung, V.Q. Tru, D.T. Luat, Static analysis of FGM cylindrical shells and the effect of stress concentration using quasi-3D type higher-order shear deformation theory, Composite Structures, 262 (2021) 113357.
[38] H. Chung, Free vibration analysis of circular cylindrical shells, Journal of Sound and Vibration, 74(3) (1981) 331-350.
[39] S. Sun, D. Cao, Q. Han, Vibration studies of rotating cylindrical shells with arbitrary edges using characteristic orthogonal polynomials in the Rayleigh–Ritz method, International Journal of Mechanical Sciences, 68 (2013) 180-189.
[40] C.L. Dym, Some new results for the vibrations of circular cylinders, Journal of sound and Vibration, 29(2) (1973) 189-205.
[41] K. Forsberg, Influence of boundary conditions on the modal characteristics of thin cylindrical shells, AIAA journal, 2(12) (1964) 2150-2157.
[42] G. Galletly, J. Mistry, The free vibrations of cylindrical shells with various end closures, Nuclear Engineering and Design, 30(2) (1974) 249-268.
[43] N.D. Duc, P.D. Nguyen, N.D. Khoa, Nonlinear dynamic analysis and vibration of eccentrically stiffened S-FGM elliptical cylindrical shells surrounded on elastic foundations in thermal environments, Thin-walled structures, 117 (2017) 178-189.